THE JOURNAL OF BIOLOGICAL CHEMISTRY VOL. 287, NO. 33, pp. 27959–27970, August 10, 2012

^{13}C-flux Analysis Reveals NADPH-balancing Transhydrogenation Cycles in Stationary Phase of Nitrogen-starving *Bacillus subtilis*[*][S]

Received for publication, March 26, 2012, and in revised form, June 3, 2012 Published, JBC Papers in Press, June 27, 2012, DOI 10.1074/jbc.M112.366492

Martin Rühl[‡§], Dominique Le Coq[¶‖], Stéphane Aymerich[¶‖], and Uwe Sauer[‡1]**

*From the [‡]Institute of Molecular Systems Biology, ETH Zurich, CH-8093 Zurich, Switzerland, [§]Life Science Zurich Graduate School, Zurich, Switzerland, [¶]INRA, Institut Micalis (UMR 1319), F-78350 Jouy-en-Josas, France, [‖]AgroParisTech, Institut Micalis (UMR), F-78350 Jouy-en-Josas, France, and **CNRS, F-78350 Jouy en Josas, France*

Background: Metabolic pathway operation and NAPDH homeostasis in non-growing bacteria is unknown.
Results: Jointly with known metabolic reactions newly discovered metabolic cycles balance the catabolic NADPH production.
Conclusion: We propose the first quantitative NADPH balancing model under non-growing conditions.
Significance: NADPH balancing is significantly different between resting and growing bacteria, reflecting microbial survival strategies during environmental challenges.

In their natural habitat, microorganisms are typically confronted with nutritional limitations that restrict growth and force them to persevere in a stationary phase. Despite the importance of this phase, little is known about the metabolic state(s) that sustains it. Here, we investigate metabolically active but non-growing *Bacillus subtilis* during nitrogen starvation. In the absence of biomass formation as the major NADPH sink, the intracellular flux distribution in these resting *B. subtilis* reveals a large apparent catabolic NADPH overproduction of 5.0 ± 0.6 mmol·g^{-1}·h^{-1} that was partly caused by high pentose phosphate pathway fluxes. Combining transcriptome analysis, stationary ^{13}C-flux analysis in metabolic deletion mutants, ^{2}H-labeling experiments, and kinetic flux profiling, we demonstrate that about half of the catabolic excess NADPH is oxidized by two transhydrogenation cycles, *i.e.* isoenzyme pairs of dehydrogenases with different cofactor specificities that operate in reverse directions. These transhydrogenation cycles were constituted by the combined activities of the glyceraldehyde 3-phosphate dehydrogenases GapA/GapB and the malic enzymes MalS/YtsJ. At least an additional 6% of the overproduced NADPH is reoxidized by continuous cycling between ana- and catabolism of glutamate. Furthermore, *in vitro* enzyme data show that a not yet identified transhydrogenase could potentially reoxidize ~20% of the overproduced NADPH. Overall, we demonstrate the interplay between several metabolic mechanisms that concertedly enable network-wide NADPH homeostasis under conditions of high catabolic NADPH production in the absence of cell growth in *B. subtilis*.

Bacteria are continuously confronted with changing environmental conditions and have therefore evolved a rich repertoire of metabolic pathways to utilize the energy and elemental sources necessary to ensure survival and promote growth (1). A frequent environmental condition is depletion of essential nutrients that causes populations to enter a so-called stationary phase (2). Several stationary phase phenomena such as persistence (3), increased stress resistance (4, 5), and, in the case of *Bacillus subtilis*, differentiation into spores (6) are the focus of intense research. Metabolism of stationary phase cells, in contrast, is not well characterized, although we generally know that cells do not shut down their metabolism but typically continue to consume energy sources when absence of other essential nutrients precludes growth (7). This metabolically active but non-growing state is referred to as resting cells (8) and is expected to play an important role in ecological processes (9).

This resting state with carbon excess can be induced by depleting any essential chemical element, but occurs most frequently in response to limited supply of the macroelements nitrogen and phosphate and the trace element iron. For the common soil bacterium *B. subtilis*, nitrogen frequently limits growth because its availability depends, among others, on climate, soil properties, constraints to biological nitrogen fixation, decomposition of litter and competition with other species (10–13). Experimentally, carbon excess conditions are typically studied in continuous cultures under nitrogen or phosphate limitation (14, 15), often using ^{13}C-flux analysis to characterize intracellular metabolism (16–18). In contrast to these still growing cultures, however, essentially nothing is known about the magnitude and distribution of metabolic fluxes in resting cells. How are the consumed carbon and energy sources catabolized and which processes recycle the generated energy and redox equivalents in the absence of biomass formation?

In principle, methods of ^{13}C-flux analysis allow to quantify energy, redox cofactor, and biosynthetic building blocks fluxes (19, 20). The vast majority of the current ^{13}C-flux methods, however, are applicable only to growing cells because the ^{13}C-labeling patterns are detected in protein-bound amino acids (21–23). As there is little or no *de novo* protein biosynthesis in resting cells, we used a recently developed mass spectrometry

* This work was supported by European Union BaSysBio Program Grant LSHG-CT-2006-037469.
[S] This article contains supplemental Tables S1–S3 and Figs. S1–S6.
[1] To whom correspondence should be addressed: Inst. of Molecular Systems Biology, ETH Zurich, 8093 Zurich, Switzerland. Tel.: 41-44-633-36 72; Fax: 41-44-633-10-51; E-mail: sauer@imsb.biol.ethz.ch.

TABLE 1
***B. subtilis* strains**

Strain	Genotype	Source or Ref.
168CA[a]	Wild-type, *trpC2*	Laboratory stock
BSB168[b]	Wild-type	*trp*+ derivative of Marburg 168 (64)
BBA9006	P_{gapB}-*gfp*/*spec*	65
GM1500	*trpC2 gapB*′::*pMUTIN2(ery)*	32
GM1608	*trpC2 ytsJ*′::*pEC23-kan*	41
GM2975	Δ*yqfI*::*phleo*	chr. DNA PS1632 (49) → BSB168
GM2976	Δ*yqfI*::*phleo*, P_{gapB}-*gfp*/*spec*	chr. DNA PS1632 (49) → BBA9006
GTD107	*trpC2 gapB*′::*pMUTIN(ery) ytsJ*′::*pEC23-kan*	chr. DNA GM1500 → GM1608
PS1679	*trpC2* Δ *(ccpN-yqfL)*::*phleo*	49

[a] Used strain for transcript analysis, enzyme assays, and ^{13}C- and ^{2}H-labeled experiments.
[b] Used strain for monitoring kinetics of P_{gapB} promoter activity.

(MS) method that detects the ^{13}C-labeling patterns directly in metabolic intermediates (24). An advantage over previous techniques (25–29) is that we detect the ^{13}C-labeling pattern not only in intact but also in fragmented carbon backbones of the intermediates that reveal indispensable intramolecular ^{13}C-label positions for stationary ^{13}C-flux analysis (19, 22, 30). We apply this new LC-MS/MS method to quantify intracellular fluxes in nitrogen starvation-induced resting *B. subtilis* cultures. In particular, we focus on the question of how *B. subtilis* recycles its catabolic NADPH formation in the absence of anabolic NADPH requirements? To identify potential NADPH consuming processes during nitrogen starvation, we started from genome-wide transcriptome data and tested various emerging hypotheses with stationary ^{13}C-flux analysis of metabolic deletion mutants, specific ^{2}H-labeling experiments, and *in vitro* enzyme assays. Therefore, we quantified the contribution of different NADPH consuming mechanisms that enable *B. subtilis* to counteract an apparent NADPH overproduction and ensure redox homeostasis.

EXPERIMENTAL PROCEDURES

Bacterial Strains, Growth Conditions, and Media—The strains used in this study are listed in Table 1. For all experiments, frozen glycerol stocks were used to inoculate 5 ml of Luria-Bertani (LB) medium, supplemented when required with 0.5 mg liter^{-1} erythromycin, 5 mg liter^{-1} kanamycin, 100 mg liter^{-1} spectinomycin, or 0.25 mg liter^{-1} phleomycin. After 5 h of incubation at 37 °C and 300 rpm on a gyratory shaker, 5 ml of M9 minimal medium was inoculated at 1000- to 4000-fold dilutions as precultures. M9 medium precultures at optical densities at 600 nm (A_{600}) of 1–2 were then used to inoculate a 70-ml M9 batch culture in a 1-liter baffled shake flask to a maximal A_{600} of 0.03. The M9 minimal medium consisted per liter of deionized water: 8.5 g of $Na_2HPO_4{\cdot}2\ H_2O$, 3.0 g of KH_2PO_4, 1 g of NH_4Cl, 0.5 g of NaCl and was adjusted to pH 7 before filter sterilization. The following components were filter sterilized separately and then added (per liter of final medium): 1 ml of 1 M $MgSO_4$, 1 ml of 0.1 M $CaCl_2$, 1 ml 0.05 M $FeCl_3$ containing 0.1 M citric acid, 20 ml of glucose 25% (w/v), 1 ml of tryptophan 5% (w/v), and 10 ml of a trace element solution containing (per liter) 170 mg of $ZnCl_2$, 100 mg $MnCl_2{\cdot}4H_2O$, 60 mg of $CoCl_2{\cdot}6H_2O$, 60 mg $Na_2MoO_4{\cdot}2H_2O$, and 43 mg $CuCl_2{\cdot}2H_2O$.

For nitrogen starvation, a M9 batch culture was grown in a shake flask to an A_{600} between 1.5 and 2, and 50 ml of culture broth were centrifuged for 1 min at room temperature and 15 min at 500 × *g*. The supernatant was discarded, and residual liquid removed by tapping on paper tissue, followed by immediate resuspension of the cell pellet in 25 ml of nitrogen starvation medium, transfer to a 500-ml flask and incubation at 37 °C and 300 rpm on a gyratory shaker. The nitrogen starvation medium contained per liter of deionized water: 8.5 g of $Na_2HPO_4{\cdot}2\ H_2O$, 3.0 g of KH_2PO_4, 0.5 g of NaCl and adjusted pH 7. The following components were added separately (per liter of final medium) 10 ml of 1 M $MgSO_4$, 10 ml of 0.1 M $CaCl_2$, and 20 ml of glucose 25% (w/v), followed by filter sterilization. M9 minimal medium and nitrogen starvation medium had the same ionic strength and were used with 5 g/liter final glucose concentration, if not stated differently.

For the ^{13}C-labeled enrichment experiment in resting cells, 100% [U-^{13}C]glucose (>99% isotopic purity; Cambridge Isotope Laboratories, Andover, MA) was added to a nitrogen starving *B. subtilis* culture growing initially on 4 g/liter naturally labeled glucose for 1.5 h. At the time of ^{13}C-tracer addition, a final mixture of 50% (w/w) [U-^{13}C] and 50% naturally labeled glucose at a final concentration of 6.8 g/liter was obtained to ensure a good response of all isotopologues in LC-MS/MS analysis. The enrichment experiment was conducted in a bioreactor at 37 °C and 0.1 bar of overpressure with a volume of 0.7 liters in a 1.5-liter vessel (Bioengineering AG, Wald, Switzerland), equipped with pH, temperature, dissolved oxygen probes, exhaust gas analyzer (GA4, DASGIP AG, Jülich, Germany), and a mass flow controller (red-y smart controller GSC, Vögtlin Instruments AG, Aesch, Switzerland). A constant airflow with 1 volume per volume and minute and an agitation speed of 1000 rpm was set to ensure dissolved oxygen levels above 50% throughout the process.

For ^{13}C-flux analysis, a mixture of 80% (w/w) [1-^{13}C] and 20% (w/w) [U-^{13}C]glucose was used (both >99% isotopic purity; Cambridge Isotope Laboratories, Andover, MA). This mixture was chosen to provide meaningful data to resolve the flux branching between glycolysis and pentose phosphate pathway from the positional label in [1-^{13}C]glucose and to resolve the tricarboxylic acid (TCA) cycle flux from the uniformly labeled [U-^{13}C]glucose (22). For deuterium labeling experiments, 100% [4-^{2}H]glucose was used (>99% isotopic purity; Omicron Biochemicals, South Bend, IN).

Physiological Parameters and Enzymatic Assays—Cell growth was determined spectrophotometrically at 600 nm. Glucose, acetoin, citrate, α-ketoglutarate, succinate, fumarate, malate, pyruvate, and acetate concentrations in the supernatant were measured by the signals of a refractive index and diode array

detector on a HPLC (Agilent 1100), using a Aminex HPX-87H column at a temperature of 60 °C with 5 mM H_2SO_4 as eluent. Supernatant samples were prepared by centrifugation of 1 ml of culture broth for 3 min at 4 °C and 14,000 × *g*. Specific growth rates were calculated by linear regression of A_{600} over time. Specific uptake and secretion rates were calculated by linear regression of consumed substrate or product concentration *versus* biomass concentration. Cell viability was estimated by plating dilutions of culture aliquots on LB solid medium and colony counting after 18 h of incubation at 37 °C. The sporulation frequency was estimated by determining the proportion of heat-resistant colony forming units with the same method, except that the culture sample was incubated 15 min at 80 °C before plating the different dilutions. Both viability and sporulation frequency were determined just before, 3 h after, and 18 h after induction of nitrogen starvation.

For enzymatic assays of glyceraldehyde-3-phosphate dehydrogenase and transhydrogenase activity, cells were harvested during mid-exponential growth of batch cultures or after ~5.5 h of nitrogen starvation by centrifugation at 4 °C and washed twice with 0.9% NaCl. Biomass pellets were kept at −80 °C until further analysis. For disruption, cells were 10-fold concentrated in lysis buffer (100 mM Tris-HCl, pH 7.5, 5 mM $MgCl_2$, 1 mM dithiothreitol, and 4 mM PMSF) and twice passed through a French press cell at 4 °C. Cell-free lysates were obtained by centrifugation at 23,000 × *g* and 10 min at 4 °C. For the enzymatic assays, 0.1 ml of the cell-free lysate was used with reaction buffer in a total volume of 1 ml at 25 °C (31). Reaction buffers were prepared as described elsewhere (32). For glyceraldehyde-3-phosphate dehydrogenase activity, the reduction of $NAD(P)^+$ was monitored at 340 nm, whereas for transhydrogenase activity, reduction of 3-acetylpyridine adenine dinucleotide$^+$ and oxidation of NADPH were spectrophotometrically measured at 400 and 310 nm simultaneously to exclude interferences in the adsorption of both NADPH and 3-acetylpyridine adenine dinucleotide (31). Protein concentration was determined using Coomassie Plus Protein Reagent (Pierce) according to the manufacturer's instructions.

Transcript Sampling and Data Analysis—For transcript analysis, cultures were grown in duplicate to the desired A_{600} with <10% deviation in A_{600} as described above. Samples for mRNA extraction were prepared by adding 30 ml of culture broth to 15 ml of crushed ice filled with killing buffer containing 20 mM Tris-HCl at pH 7.5, 5 mM $MgCl_2$, and 20 mM NaN_3. For rapid harvest, this mixture was centrifuged for 3 min at 8300 × *g* and 4 °C, the supernatant immediately discarded and cells frozen in liquid N_2 and stored at −80 °C.

RNA extraction was performed precisely as described elsewhere (33). For labeling and hybridization, we used the strand specific conditions by NimbleGen as described by Rasmussen *et al.* (34), and raw data treatment was done as described by Nicolas *et al.* (35). We used MultiExperiment Viewer software MeV (version 4.6.1) for principal component analysis. Differential analysis was carried out separately for each comparison between the two culture conditions, by considering only genes with 2-fold or more differential expression at a threshold of 5-fold above background expression (*i.e.* a value of 1000) under at least one condition.

Mass Spectrometric ^{13}C-labeling Pattern Analysis—For quantification of ^{13}C-labeling pattern in metabolic intermediates, rapid quenching of metabolic activity was necessary to avoid artifacts caused by the high exchange rates and small pool sizes of metabolites (19, 36). For this purpose, 10 ml of culture broth of mid-exponential batch cultures or nitrogen starving resting cultures after a 5.5-h incubation were mixed with 40 ml of an aqueous −40 °C cold 60% (v/v) methanol solution containing 10 mM ammonium acetate, pH 7.5 (37), directly followed by centrifugation at −20 °C and 15,500 × *g* for 1 min. The supernatant was immediately removed, and cell pellets were frozen in liquid nitrogen. To assure sufficient biomass between 10 and 20 mg cell dry weight for extraction, two 10-ml culture aliquots were independently quenched and pooled.

To extract metabolites, quenched cell pellets were extracted three times with 0.5 ml of a 78 °C hot 60% (v/v) aqueous ethanol solution containing 10 mM ammonium acetate for 1 min and centrifuged at −10 °C for 3 min at 14,000 × *g*. The pooled extracts were dried in a SpeedVac at 0.12 millibars and 30 °C and stored at −80 °C until further analysis. For subsequent LC-MS/MS analysis of isotopologue distributions, dried pellets were resuspended in 60 μl of deionized water, 8 μl of which were injected into using conditions published elsewhere (24).

For ^{13}C-labeling pattern analysis in free intracellular amino acids by gas chromatography (GC) MS, the obtained metabolite extract was further processed following a previously established protocol (24). Briefly, after drying the ethanolic extract in a vacuum centrifuge, 20 μl of dimethylformamide (Fluka, Switzerland) was added. After resuspension, 15 μl of supernatant was used with 15 μl of *N*-(tert-butyldimethylsilyl)-*N*-methyltrifluoroacetamide (Sigma) for derivatization at 85 °C for 1 h. For analysis of ^{13}C-patterns in derivatized amino acids, published GC-MS settings were used (22).

^{13}C-constrained Metabolic Flux Analysis—To estimate intracellular carbon fluxes, we used network-wide stationary isotopologue balancing (22, 38). This procedure relies on the steady state ^{13}C-pattern in metabolic intermediates that we obtained by LC-MS/MS (24) and measured extracellular rates of substrate consumption and product formation. These measured data are quantitatively connected to intracellular fluxes through a stoichiometric model of atom transitions between metabolic intermediates in central metabolism (*i.e.* an isotopologue model). The network-wide distribution of intracellular fluxes was then estimated indirectly with a computational procedure that iteratively improves the fit between simulated mass isotope patterns and extracellular rates and the actually measured data. For the model, we used the recently published reaction reversibilities for *B. subtilis* (39). The publicly available software 13CFLUX (38) was used for flux computation and error estimation, following the principles of model construction, fitting, quality evaluation of the obtained fit, and error estimation described elsewhere in a detailed step-by-step tutorial (22). The ^{13}C-flux fits were independently verified through ^{2}H-label experiments, enzyme assays, and transcriptome data. To calculate NADPH production, we summed the estimated carbon fluxes through the NADPH-dependent reactions of glucose-6-phosphate dehydrogenase (Zwf), the 6-phosphogluconate dehydrogenase isoenzyme (GndA) (40), isocitrate dehy-

TABLE 2
Physiological data of nitrogen starvation-induced resting *B. subtilis* wild-type and mutant cultures at 5.5 h after resuspension

Strain	Glucose uptake rate[a]	Specific production rates		
		Acetoin	Citrate	Others[b]
	mmol·g⁻¹·h⁻¹		*mmol·g⁻¹·h⁻¹*	
Wild-type[c]	1.92	0.83	0.25	0.09
Wild-type[d]	1.99	0.82	0.28	0.09
gapB[d]	2.32	1.06	0.41	0.16
ytsJ[d]	1.97	0.94	0.20	0.11
gapB/*ytsJ*[d]	1.63	0.49	0.69	0.09

[a] Errors were estimated from two independent wild-type experiments to be within 5% for glucose uptake and acetoin production rate, and within 10% for citrate and the other TCA cycle intermediates.
[b] Shown are the summed secretion rates of the TCA cycle intermediates α-ketoglutarate, succinate, fumarate, and malate. Acetate and pyruvate were not produced.
[c] Wild-type strain was grown in bioreactor. Based on the physiological rates and a CO_2 production rate of 6.04 mmol·g^{-1}·h^{-1} in this bioreactor experiment, the carbon balance closed to 98%.
[d] Strains were grown in shake flask cultures.

drogenase (Icd), and initially also malic enzyme isoenzyme (YtsJ) (41), assuming 100% specificity for $NADP^+$, except for Zwf and GndA that were recently shown to be only ~90% specific (31).

Kinetics of gapB Derepression upon Shift to Nitrogen Starvation—Strains carrying a P_{gapB}-*gfpmut3* transcriptional fusion were grown under vigorous shaking at 37 °C in test tubes with M9 medium until an A_{600} of about unity. After centrifugation, cells were immediately resuspended to the same A_{600} in either the same medium or in medium lacking the nitrogen source. 100 μl of these resuspensions were placed in 96-well cell culture plates (CELLSTAR, Greiner bio-one) and incubated under constant shaking at 37 °C in a SynergyTM II microplate reader (Biotek). The A_{600} and fluorescence (excitation, 485/20 nm; emission, 528/20 nm) were measured every 7 min in triplicate cultures. After correction for medium background fluorescence and autofluorescence of the parental strain (*i.e.* without the P_{gapB}-*gfpmut3* fusion), *gapB* promoter activity was estimated from the GFP concentration measured as fluorescence units per A_{600} at each time point.

RESULTS

Steady State Physiology in Nitrogen Starvation-induced Resting B. subtilis—To characterize metabolism in nitrogen starving, resting *B. subtilis* without *de novo* biomass formation, we grew the wild-type strain in a bioreactor batch culture in glucose minimal medium until mid-exponential phase to an A_{600} of 1.6. Upon harvesting and resuspending in fresh medium without a nitrogen source, the culture immediately ceased to grow (supplemental Fig. S1) but maintained metabolic activity with a constant glucose uptake rate of 1.9 mmol·g^{-1}·h^{-1} for at least 5.5 h (Table 2), *i.e.* 23% of the uptake rate during exponential growth with 8.2 mmol·g^{-1}·h^{-1} (Fig. 1) (24).

These physiological data suggested a quasi steady state during nitrogen starvation. To determine the time required for metabolic intermediates to attain isotopic stationarity for ^{13}C-flux analysis, we added uniformly labeled [U-^{13}C]glucose to the resting culture ~1.5 h after entry into starvation. Because this ^{13}C-tracer addition resulted in a final mixture of 50% [U-^{13}C] and 50% naturally labeled glucose in the medium (supplemental Fig. S1), one hence expects 0.50 ± 0.02 fractional labeling and stable isotopologue distributions in all metabolic intermediates at isotopic steady state. As expected from similar experiments (42–45), we observed different dynamics of label enrichment that were a function of metabolite pool size, fluxes, and the metabolic distance to the label entry (supplemental Fig. S2). Within 3 min, the most rapid isotopic steady state was achieved by glucose-6-phosphate, followed by the intermediates of glycolysis and pentose phosphate pathway within ~10 min. TCA cycle intermediates exhibited the slowest label enrichment, reaching 95% of the input fractional labeling after 200 min. This isotopologue buffering is probably caused by label exchange with the large pool of unlabeled free amino acids through the transamination reactions of glutamate and aspartate (supplemental Fig. S2) (44, 45). To ensure quasi isotopic stationarity, all of the following ^{13}C-experiments with resting cells were therefore conducted for at least 5.5 h.

^{13}C-flux Analysis Reveals Large NADPH Overproduction in Resting Wild-type B. subtilis—Based on the quasi steady state conditions for nitrogen starvation-induced resting *B. subtilis*, we quantified absolute intracellular carbon fluxes by network-wide stationary isotopologue balancing (22, 38). In this procedure, an intracellular distribution of fluxes is indirectly estimated *in silico* from measured ^{13}C-patterns and physiological rates as a best fit to the experimental data with a detailed stoichiometric model of atom transitions in metabolism. Because only little *de novo* protein biosynthesis occurs in resting cells, we could not rely on standard flux methods (19, 36) that detect ^{13}C-patterns in proteinogenic amino acids and instead determined ^{13}C-patterns of intact and fragmented carbon backbones by targeted LC-MS/MS in metabolic intermediates (24). Exponentially growing shake flask cultures were harvested and resuspended in nitrogen starvation medium containing a mixture of 80% (w/w) [1-^{13}C] and 20% (w/w) [U-^{13}C]glucose that is well suited to resolve glucose fluxes in central carbon metabolism consisting of glycolysis, pentose phosphate pathway, TCA cycle, and anaplerotic and gluconeogenic reactions (22). Judged by the consistent physiological rates in bioreactor and shake flasks, both culture conditions were equivalent (Table 2).

Flux computation based on network-wide isotopologue balancing with ^{13}C-labeling pattern of intermediates (supplemental Table S1) revealed the relative distribution of intracellular fluxes in resting cells to be entirely different from the distribution in exponentially growing cultures (Fig. 1) (24). Although the absolute glycolytic flux was ~4-fold lower, the relative flux into the TCA cycle was 4-fold increased, and significant futile, ATP-dissipating cycling occurred in the phosphoenolpyruvate, pyruvate, and oxaloacetate triangle of resting cells. The latter two features were also described for very slowly growing carbon- or nitrogen-limited continuous cultures of *B. subtilis* (17, 45). Rather surprisingly, however, we observed an extraordinarily high flux of 64% of the consumed glucose into the pentose phosphate pathway (Fig. 1*B*), a pathway normally considered to supply pentoses and NADPH for biomass formation that does not occur in our resting cultures. Summing up all NADPH-producing fluxes through the two reactions of the oxidative pentose phosphate pathway, isocitrate dehydrogenase in the TCA cycle and malic enzyme, the data revealed a large catabolic NADPH production of 5.0 ± 1.5 mmol·g^{-1}·h^{-1} (Fig. 1*B* and

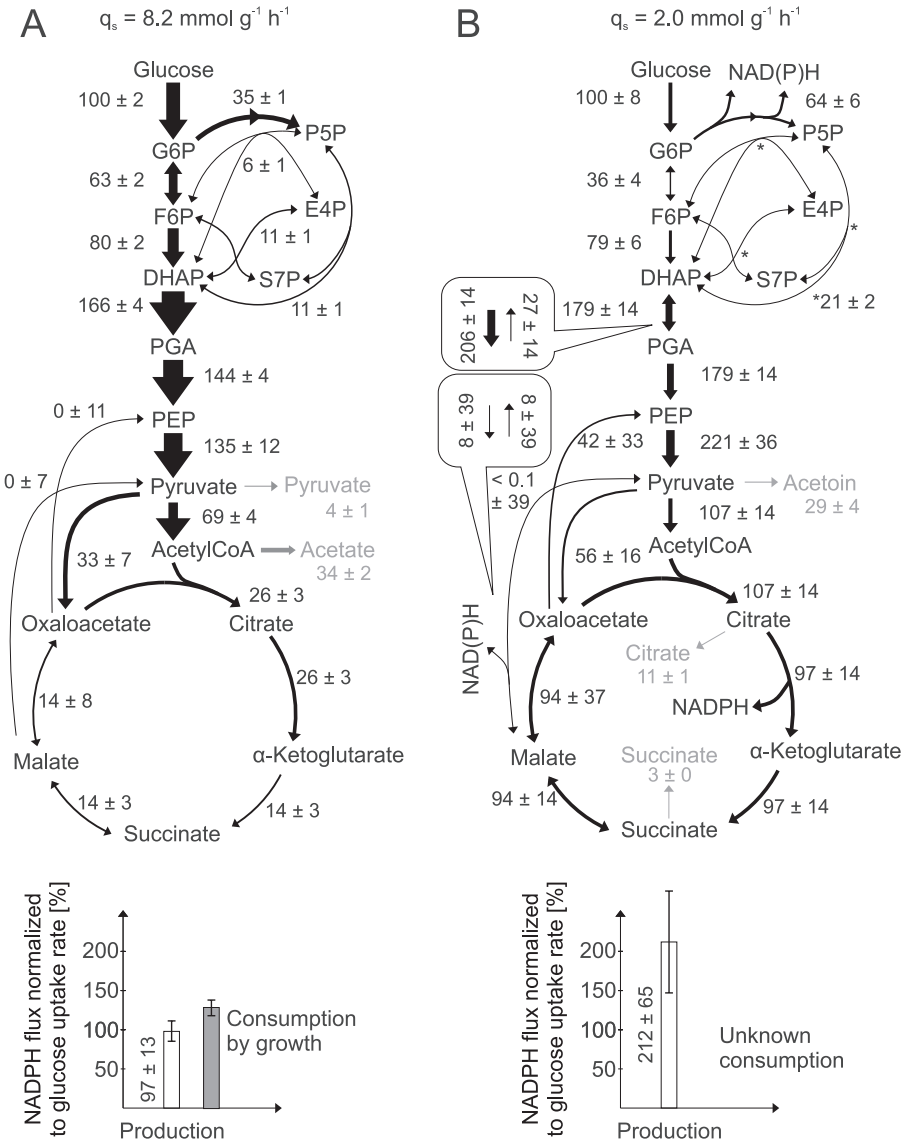

FIGURE 1. **Relative distribution of intracellular fluxes in exponentially growing batch (*A*) and nitrogen starvation-induced resting *B. subtilis* cultures (*B*).** The ^{13}C-labeling experiment was performed with 20% (w/w) [U-^{13}C] and 80% (w/w) [1-^{13}C]glucose, using LC-MS/MS for ^{13}C-pattern determination in metabolic intermediates. Flux values are normalized to the specific glucose uptake rate of each culture, whereas *arrow sizes* are relative to the glucose uptake rate of batch-grown *B. subtilis* wild-type. *Boxes* refer to the estimated forward and backward fluxes. *Errors* are S.D. obtained from error propagation using multivariate statistics (22, 38). *G6P*, glucose 6-phosphate; *DHAP*, dihydroxyacetone phosphate; *E4P*, erythrose 4-phosphate; *F6P*, fructose 6-phosphate; *PGA*, phosphoglycerate; *PEP*, phosphoenolpyruvate; *P5P*, pentose 5-phosphate; *S7P*, sedoheptulose 7-phosphate.

supplemental Table S1). In contrast to exponential growing cells, however, it is unclear how this catabolic NADPH flux is reoxidized to $NADP^+$. Indeed, in the absence of *de novo* biomass formation as the major NADPH sink, so far unknown mechanisms must operate in resting cells to balance NADPH formation and consumption (Fig. 1).

Transcriptional Analysis in Nitrogen Starvation-induced Resting B. subtilis—To identify such potential NADPH-consuming processes in resting *B. subtilis*, we compared the transcriptome of exponential growing and nitrogen-starving cultures. Of 5737 measured transcript levels, ~40% changed significantly during starvation with 1290 transcripts being at least 2-fold down-regulated and 1099 transcripts being at least 2-fold up-regulated (supplemental Fig. S3 and Table S2). There was no indication of a general stress response because 131 of the 156 measured transcripts in the σ^B-dependent general stress regulon (4) did not change or were even down-regulated (supplemental Table S2). Likewise, we found no indication of an oxidative stress response because none of the 20 genes that are known to respond to oxidative stress induced by hydrogen peroxide or paraquat (46), including the katalase-coding *katA* gene, were significantly induced in resting cells (supplemental Fig. S4). Several of the genes that are subject to stringent control (47) were also differentially expressed in nitrogen starvation-induced resting cells, although often to a lesser extent. Moreover, some genes of the RelA regulon were repressed in nitrogen starvation-induced resting cells, although they are under a positive stringent control in amino acid starvation conditions (*e.g.* the *ilvBHC/leuABCD* operon, *ilvK* (*ywaA*), *ald*, *adeC*). This confirmed that both starvation conditions are not equivalent and induce specific, but partially overlapping, responses (48). Although some sporulation genes were up-regulated, there was

no coordinated sporulation expression pattern, and sporulation frequency remained low (~1% of the colony forming units) during several hours (supplemental Fig. S5).

As can be expected from an economic response to reduce biosynthesis and to liberate nitrogen-containing compounds that are not required under nitrogen starvation, we observed two pronounced metabolic gene expression responses: (i) an overall down-regulation of biosynthesis pathways, and (ii) up-regulation of genes involved in uptake, salvage, or degradation of intra- and extracellular nitrogen sources. Generally, these results are consistent with an incomplete set of expression data from the transition of exponential growth to nitrogen starvation (48). The general biosynthetic down-regulation upon nitrogen starvation affected all pathways to the major biomass constituents. The pyrimidine and purine biosynthesis (*i.e.* the *pyrRPBC*/*AA*/*AB*/*KDFE* and *purEKBCSQLFMNHD* operons, and the *pyrG*, *pyrH*, *purA*, *purT*, *guaA*, and *guaC* genes) were almost completely shut-off. Similarly, a strong down-regulation was seen for the biosynthesis pathways to the cell wall components peptidoglycan (*mur* genes) and teichoic acid (*dlt*, *gga*, *gta* but not the *tag* genes) and to vitamins and cofactors, *e.g.* biotin (*bioWKFDBI*), NAD (*nadBCA* operon, *nadE*, *nadR*, and *nifS*), pyridoxal phosphate (*pdxK*), and thiamin (*thiC*). Although most amino acid biosynthesis genes were >2-fold down-regulated, genes for arginine, asparagine, glutamine, and threonine biosynthesis remained unchanged or were even up-regulated. Despite the general down-regulation of biosynthesis genes, the majority of them were still expressed above the background level.

The expected up-regulation of genes for utilization of extracellular nitrogen sources included the low affinity ammonium transporter *amtB* (*nrgA*), the *nas* genes for utilization of nitrate/nitrite, the *dpp* genes for degradation/uptake of cell wall peptides, and the *app*/*opp* genes for oligopeptide uptake (supplemental Table S2). Up-regulation of nucleotide degradation and salvage pathways included the purine salvage (*adeC*, *adk*, *apt*, *deoD*, *gmk*, *guaD*, *hprT*, *ndk*, *nrdE*, *nrdF*, *pupG*, *purA*, *purB*, *xpt*) and degradation pathway genes (*deoD*, *pupG*, *drm*, *dra*, *puc*, and *ureABC*) (supplemental Table S2). Strikingly, the *pucABCDE* operon was induced from a silent state during exponential growth to the highest absolute transcription signal value observed under nitrogen starvation. In contrast to nucleotides, amino acid degradation exhibited a rather heterogeneous response. Although the asparagine, glutamine, proline and serine degradation genes were typically 2- to 5-fold induced, alanine and aspartate degradation genes were 2- to 4-fold down-regulated, and glycine, isoleucine, leucine, and valine degradation gene expression was virtually shut off. The remaining amino acid degradation genes remained at their exponential growth expression level that was moderate for arginine and very low for glutamate, histidine, threonine, and cystine.

Consistent with the overall reduced metabolic activity in nitrogen starvation-induced resting compared with exponentially growing *B. subtilis* (Fig. 1 and Fig. 2*A*), important glycolytic genes such as the *ptsGHI* operon (3–27-fold), the large *cggR-gapA-pgk-tpi-pgm-eno* operon (6–10-fold), and the pyruvate dehydrogenase-encoding *pdhABCD* operon (5–9-fold)

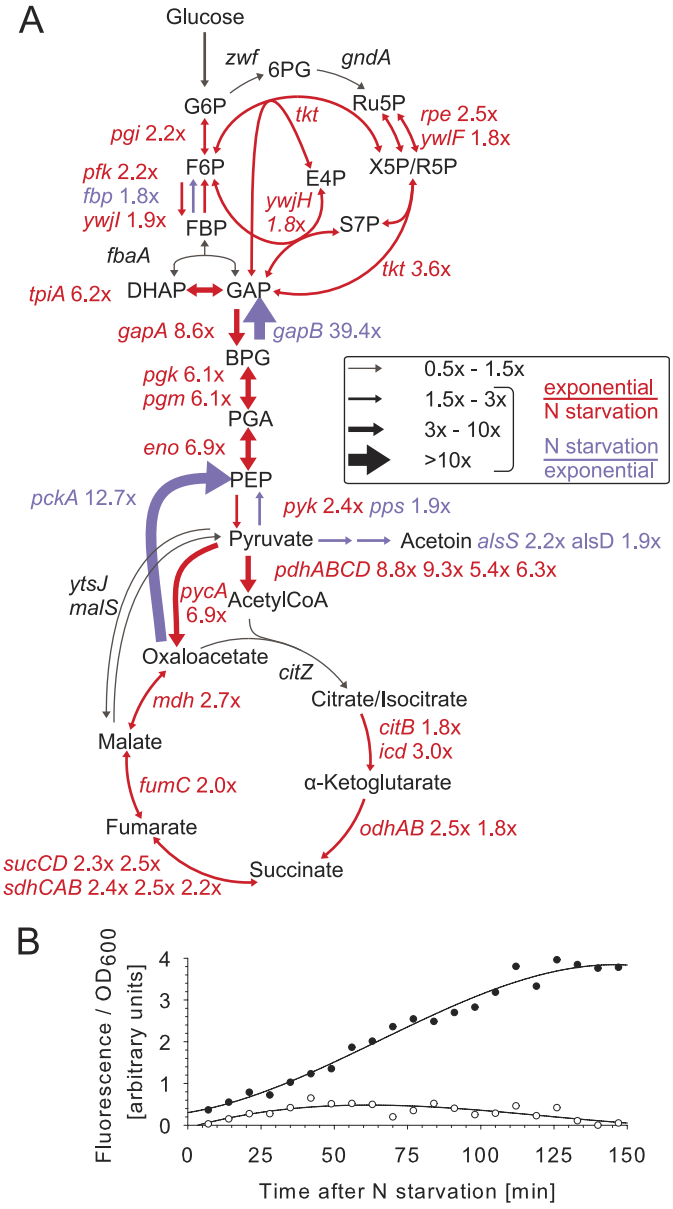

FIGURE 2. *A*, transcript fold changes in central metabolism of nitrogen starvation-induced resting compared with exponentially growing *B. subtilis* wild-type cultures. *B*, kinetics of P_{gapB} promoter activity in *B. subtilis* wild-type (*black circles*) and *yqfL* mutant (*open circles*) upon entry into nitrogen starvation of P_{gapB}-*gfp* carrying strains. *G6P*, glucose 6-phosphate; *DHAP*, dihydroxyacetone phosphate; *E4P*, erythrose 4-phosphate; *F6P*, fructose 6-phosphate; *PGA*, phosphoglycerate; *PEP*, phosphoenolpyruvate; *P5P*, pentose 5-phosphate; *S7P*, sedoheptulose 7-phosphate; *N*, nitrogen.

were essentially repressed. Likewise, the pentose phosphate pathway and TCA cycle were uniformly down-regulated 2–3-fold. Strikingly, the only up-regulated genes in central metabolism were the gluconeogenic *gapB* and *pckA* with 39- and 13-fold higher expression levels in resting cells, respectively (Fig. 2*A* and supplemental Table S2). Because these genes are normally fully repressed by CcpN in the presence of glucose during exponential growth (49, 50), nitrogen starvation appears to alleviate glucose repression, despite the presence of high glucose concentrations.

It is noteworthy that the small regulatory RNA *SR1* encoding *ykzW* gene, the only other gene known to be repressed by CcpN

under glycolytic conditions (51), was also strongly derepressed (36-fold higher expression) in resting cells (supplemental Table S2). As a positive regulator of *gapB*/*pckA*/*SR1*, YqfL had been shown to modulate CcpN repressor activity (49). Although YqfL appears to play only a modest role during exponential growth, our data[2] indicated importance of YqfL under nutritional deficiency, which led us to investigate the potential role of this regulator in derepression of *gapB*. For this purpose, we determined expression of a P_{gapB}-*gfp* reporter fusion in wild-type and *yqfL* mutant during the shift from growth into nitrogen starvation. The P_{gapB} promoter was repressed during exponential growth on glucose and strongly derepressed immediately following the shift to nitrogen starvation. This strong derepression was completely abolished in a *yqfL* mutant (Fig. 2*B*). The same YqfL-dependent derepression upon nitrogen starvation was also observed for the P_{sr1} promoter (data not shown). These results demonstrate the involvement of the YqfL regulator in the derepression.

MalS/YtsJ and GapA/GapB Transhydrogenation Cycles Contribute to NADPH Balancing During Nitrogen Starvation—Important for NADPH metabolism, simultaneous activity of the gluconeogenic, NADPH-dependent glyceraldehyde-3-phosphate dehydrogenase GapB and the glycolytic, NAD^+-dependent GapA (32) could potentially constitute a transhydrogenation cycle that interconverts the two redox equivalents. Although *gapA* was down-regulated in resting cells (Fig. 2*A*), there was still significant residual expression (supplemental Table S2). Furthermore, the ^{13}C-flux estimates indicated indeed some back-flux from 1,3-bisphosphoglycerate to dihydroxyacetone-P in resting cells (Fig. 1*B*). Because the global flux fit obtained by isotopologue balancing allows only for an indirect estimation of this exchange, we used deuterium-labeled glucose to directly assess the *in vivo* back-flux through the GapB-catalyzed reaction against the otherwise glycolytic flux in resting cells. Specifically, we chose [4-^{2}H]glucose because the deuterium atom is split off in the GapA-catalyzed reaction that yields 1,3-bisphosphoglycerate (52, 53). Hence, glycolytic intermediates above the GapA reaction should contain the ^2H-label, whereas it will be lost in 1,3-bisphosphoglycerate and downstream metabolites (Fig. 3*A*). A GapB-catalyzed *in vivo* back-flux should then reveal itself in higher relative contents of unlabeled metabolites in upper glycolysis upon feeding [4-^{2}H]glucose. Relative to the negative control of a *gapB* deletion mutant, there was indeed a 15 ± 2% higher ^2H-labeled loss in upper glycolysis metabolites (FBP, Fru-6-P, Glc-6-P) of the resting wild-type culture (Fig. 3*A*).

To exclude that the relative ^2H-labeled loss was caused by significantly different pentose phosphate pathway fluxes that transport mainly unlabeled intermediates (Fig. 3*A*), we verified similarity of fluxes between resting cultures of wild-type (Fig. 1*B*) and *gapB* mutant (Fig. 3*B*) by ^{13}C-flux analysis. In addition to very similar relative net fluxes in upper glycolysis and pentose phosphate pathway, also the estimated exchange fluxes were similar, and consistently, the global flux fit for the *gapB* mutant showed an absent GapB flux (supplemental Table S1).

[2] M. Ruhl, D. Le Coq, S. Aymerich, and U. Sauer, unpublished observations.

Finally, we confirmed GapB activity in resting wild-type cultures by *in vitro* enzyme assays with cell extracts from an exponentially growing *ccpN* mutant as a positive control (50) and the resting *gapB* mutant as the negative control (Fig. 3*C*). Because all data supported an active gluconeogenic GapB reaction in otherwise glycolytic resting *B. subtilis*, we assessed the contribution of the GapA/GapB transhydrogenation cycle to overall NADPH balancing from the apparent NADPH overproduction of the resting *gapB* mutant, again by summing up fluxes through all NADPH-generating reactions. The reduction of the apparent catabolic NADPH overproduction from 5.0 ± 1.5 $mmol \cdot g^{-1} \cdot h^{-1}$ in the wild-type to 4.7 ± 1.2 $mmol \cdot g^{-1} \cdot h^{-1}$, in the *gapB* mutant was disappointingly small and statistically insignificant (Fig. 3*B* and supplemental Table S1), suggesting that this cycle is either not relevant for redox homeostasis or that it is effectively replaced by another cycle.

A similar potential transhydrogenation cycle could consist of the NAD^+- and NADPH-dependent malic enzymes MalS and YtsJ (41) that were both expressed in resting cultures (supplemental Table S2). Akin to the GapA/GapB cycle, we quantified the NADPH balancing capacity of the putative MalS/YtsJ transhydrogenation cycle by ^{13}C-flux analysis from a 80% (w/w) [1-^{13}C] and 20% (w/w) [U-^{13}C]glucose-labeling experiment with the *ytsJ* mutant. We found only a small reduction in apparent catabolic NADPH overproduction to 4.0 ± 0.5 $mmol \cdot g^{-1} \cdot h^{-1}$ (Fig. 4*A* and supplemental Table S1). Because these results showed that the NADPH-dependent malic enzyme YtsJ operated in resting cells in the NADPH-consuming direction from pyruvate to malate, we could improve the confidence of our apparent NADPH overproduction estimate in wild-type to 5.0 ± 0.6 $mmol \cdot g^{-1} \cdot h^{-1}$ because only the pentose phosphate pathway and TCA cycle fluxes must be considered for NADPH formation (supplemental Table S1).

Because both transhydrogenation cycles might synergistically contribute to NADPH balancing or replace each other, we determined NADPH production in a nitrogen starvation-induced resting culture of the *ytsJ*/*gapB* double mutant by ^{13}C-flux analysis. Effective disruption of both transhydrogenation cycles by deleting both NADPH-dependent isoenzymes genes caused high acetoin and citrate production, indicating reduced carbon flux through the NADPH-dependent isocitrate dehydrogenase reaction (Table 2). The apparent catabolic NADPH overproduction of 2.6 ± 0.3 $mmol \cdot g^{-1} \cdot h^{-1}$ in the *ytsJ*/*gapB* double mutant was indeed significantly lower than in either single deletion mutant (Fig. 4*B* and supplemental Table S1). Thus, the combined activity of both transhydrogenation cycles was capable to balance 2.4 ± 0.3 $mmol \cdot g^{-1} \cdot h^{-1}$, about half of the apparent catabolic NADPH overproduction in resting *B. subtilis*.

NADPH Consumption through Simultaneous Anabolism and Catabolism of Amino Acids and a Transhydrogenase Reaction—How does *B. subtilis* metabolism cope with the remaining apparent NADPH overproduction of 2.6 ± 0.3 $mmol \cdot g^{-1} \cdot h^{-1}$ in wild-type? Because the transcription data suggested coexistence of *de novo* biosynthesis and degradation of amino acids, continuous cycling between the NADPH-dependent anabolism and the NAD^+-dependent catabolism could result in another NADPH-consuming mechanism (supplemental Fig. S6). If this hypothesis was true, one would expect

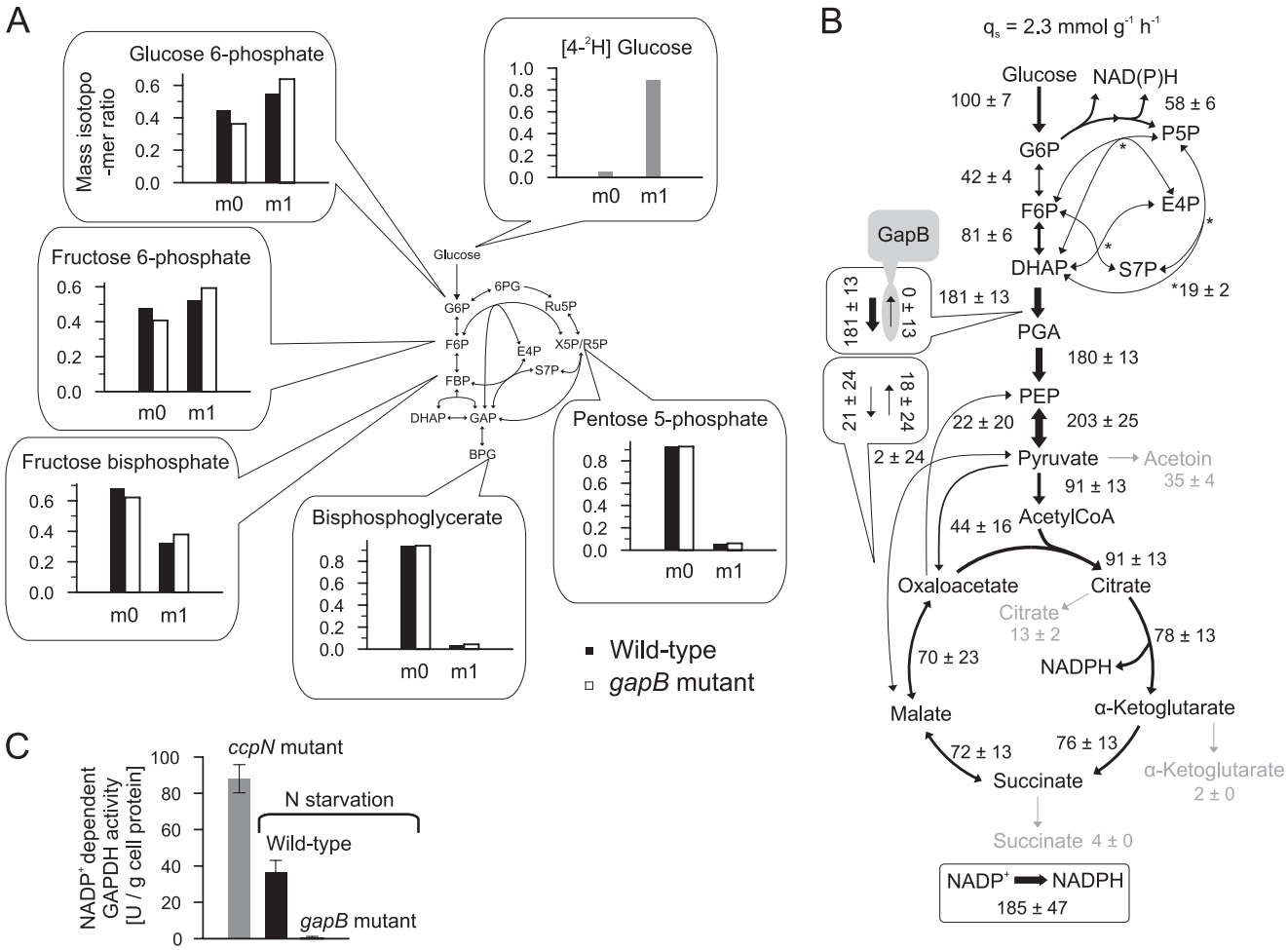

FIGURE 3. **Quasi isotopic steady state ^{2}H-labeled distribution (*A*), intracellular fluxes (*B*), and *in vitro* GapB activity (*C*) of *B. subtilis* wild-type and *gapB* mutant.** ^{2}H-Labeling was achieved by feeding 100% [4-^{2}H]glucose to resting wild-type and *gapB* deletion mutant. Unlabeled molecules are denoted as *m0*, and single ^{2}H-labeled molecules are labeled as *m1*. The relative distribution of intracellular fluxes in a nitrogen starvation-induced resting *gapB* mutant was obtained by LC-MS/MS analysis of ^{13}C-pattern in intermediates upon labeling with 20% (w/w) [U-^{13}C] and 80% (w/w) [1-^{13}C]glucose. Flux values are normalized to the glucose uptake rate, whereas *arrow size* is relative to glucose uptake rate of an exponentially growing *B. subtilis* wild-type batch culture (as shown in Fig. 1*A*). *Boxes* refer to the forward and backward fluxes. As a positive control, *in vitro* GapB activity was determined in crude cell extracts of an exponentially growing *ccpN* mutant (50), where the *error bars* represent technical replicates. *G6P*, glucose 6-phosphate; *DHAP*, dihydroxyacetone phosphate; *E4P*, erythrose 4-phosphate; *F6P*, fructose 6-phosphate; *PGA*, phosphoglycerate; *PEP*, phosphoenolpyruvate; *P5P*, pentose 5-phosphate; *S7P*, sedoheptulose 7-phosphate; *N*, nitrogen.

significant ^{13}C-labeling in certain free amino acids and their precursors in resting cells, which otherwise are expected to be unlabeled because amino acid biosynthesis is not required in the absence of cell growth. Indeed, such *in vivo* ^{13}C-labeled enrichment (supplemental Fig. S2) was found for the intermediates of one potential glutamate/aspartate cycle that consists of (i) the NADPH-consuming conversion of α-ketoglutarate to glutamate by GltAB, α-ketoglutarate regeneration through AspB-catalyzed glutamate transamination that forms aspartate from oxaloacetate, and (ii) NAD^+-dependent aspartate degradation to oxaloacetate by combined activity of ArgG, ArgH, FumC (CitG), and Mdh (Fig. 5). All involved genes were expressed in resting cells (supplemental Table S2). Actually, the genes *argG* and *argH* were ~4-fold up-regulated in resting *B. subtilis* and are part of the urea cycle that was generally up-regulated (*argJ*, 1.5×; *argB*, 1.7×; *argC*, 2.3×; *argD*, 2.0×; *argF*, 1.8×; *argG*, 4.5×; *argH*, 3.6×; *argI*, 0.7×; *ureA*, 11.2×; *ureB*, 10.4×; *ureC*, 8.2×). Additionally, other glutamate and aspartate degradation pathways are possible (supplemental Fig. S6).

Because stationary ^{13}C-flux analysis cannot determine the flux through the NADPH-consuming GltAB reaction, we used kinetic flux profiling (28) to estimate the lower bound for the net flux. To determine a reaction flux by kinetic flux profiling, the experimentally determined rate constant of ^{13}C-labeled enrichment, *i.e.* the ratio of the flux to the total pool size, is multiplied with the intracellular pool size (28). For the NADPH-consuming GltAB reaction, the rate constant was determined by fitting a first-order integrated rate equation to the measured monoisotopic mass time course of glutamate (supplemental Fig. S2), followed by multiplying this rate with the known pool size of glutamate. For the free glutamate pool with a first-order rate of 3.9 ± 0.2 h^{-1} and an averaged intracellular concentration obtained from different steady state conditions of 77.3 ± 8.6 μmol/g dry cell weight (39), a lower bound of the NADPH-consuming flux of 0.3 ± 0.1 mmol·g^{-1}·h^{-1} was calculated.

Although this flux through the GltAB reaction would only account for 6 ± 1% of the apparent catabolic NADPH overpro-

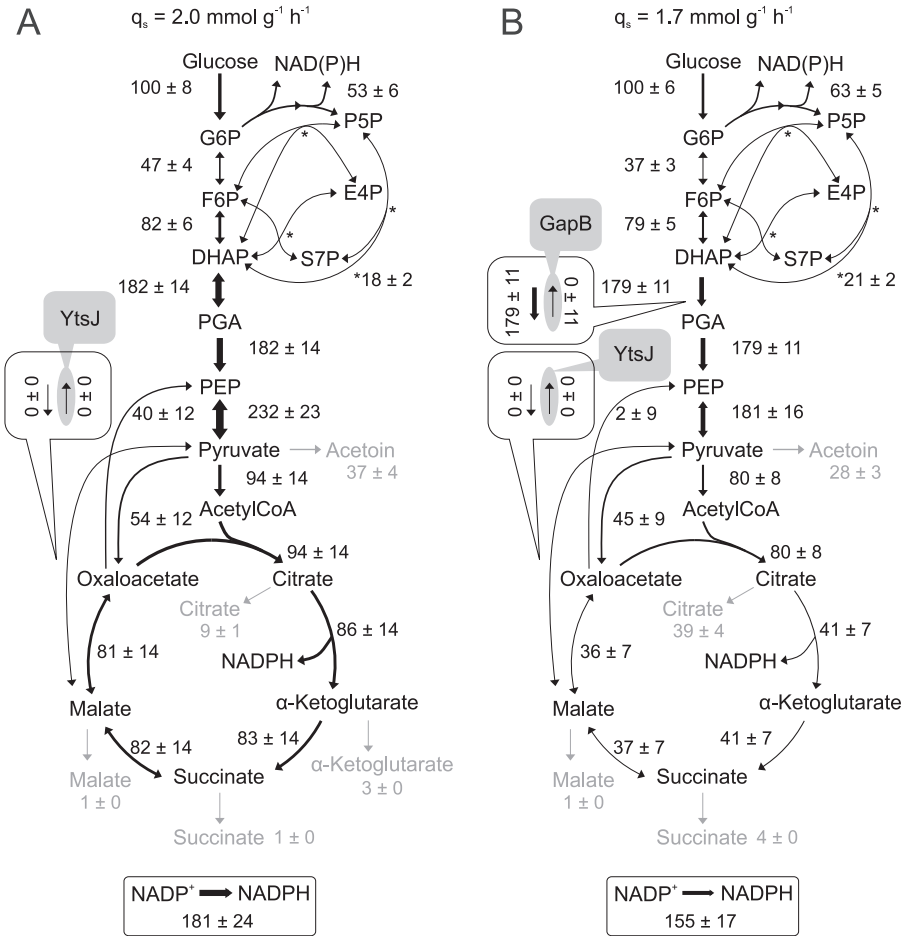

FIGURE 4. **Relative distribution of intracellular fluxes in nitrogen starvation-induced resting cultures of a *B. subtilis ytsJ* mutant (*A*) and *ytsJ*/*gapB* double mutant (*B*).** ^{13}C-Labeling pattern were detected by LC-MS/MS in metabolic intermediates from a 20% (w/w) [U-^{13}C] and 80% (w/w) [1-^{13}C]glucose experiment. Flux values are normalized to each cultures glucose uptake rate, whereas *arrow sizes* are relative to the glucose uptake rate of batch-grown *B. subtilis* wild-type (shown in Fig. 1*A*). *Boxes* refer to the forward and backward fluxes, and *gray areas* indicate the deleted enzymatic reaction. *G6P*, glucose 6-phosphate; *DHAP*, dihydroxyacetone phosphate; *E4P*, erythrose 4-phosphate; *F6P*, fructose 6-phosphate; *PGA*, phosphoglycerate; *PEP*, phosphoenolpyruvate; *P5P*, pentose 5-phosphate; *S7P*, sedoheptulose 7-phosphate.

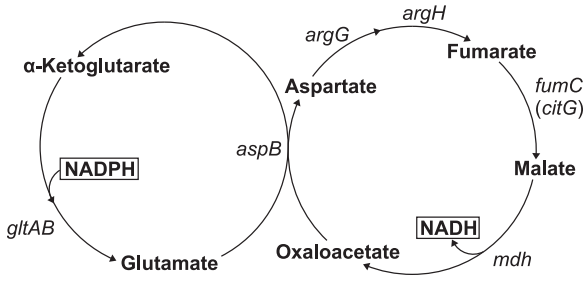

FIGURE 5. **Proposed transhydrogenation cycle of glutamate/aspartate biosynthesis/degradation in nitrogen starvation-induced resting *B. subtilis*.**

duction in resting *B. subtilis*, the overall contribution of amino acid synthesis to NADPH balancing could be significantly higher because half of the proteinogenic amino acids require NADPH for biosynthesis (supplemental Table S3 and Fig. S6). Because our LC-MS/MS data contained only labeling information for aspartate and glutamate, we determined the ^{13}C-labeled enrichment in free intracellular amino acids after 3.2 h of ^{13}C-labeling in the resting *B. subtilis* culture (supplemental Fig. S1) also by GC-MS (45). Supporting the hypothesis of significant NADPH consumption by continuous amino acid recycling, we found the free aromatic and branched chain amino acids to be significantly enriched for ^{13}C-labeling (supplemental Table S3). Due to the complexity of amino acid metabolism (supplemental Fig. S6), however, the present data do not allow for a precise quantification of the NADPH consumption by this mechanism, but the 0.3 ± 0.1 mmol·g^{-1}·h^{-1} NADPH consumption estimated for the GltAB reaction appears to be an underestimate.

Quantification of the NADPH balancing capacity of two combined transhydrogenation cycles and the coupled synthesis/degradation cycle for glutamate/aspartate still left some not yet accounted for apparent NADPH overproduction. Consequently, at least one further mechanism must exist, and the transhydrogenase reaction that directly transfers electrons from NADPH to NAD^+ is the most probable candidate (54). Although no genes were annotated for this reaction in *B. subtilis*, we found significant *in vitro* transhydrogenase activity in nitrogen starvation-induced resting wild-type that was only marginally lower in exponentially growing cells and similar in the *ytsJ*/*gapB* double mutant (Fig. 6*A*) (31, 55, 56). If this *in vitro* activity could be exploited *in vivo*, the transhydrogenase reaction could potentially contribute 1.1 ± 0.1 mmol·g^{-1}·h^{-1} or ~21% to NADPH balancing.

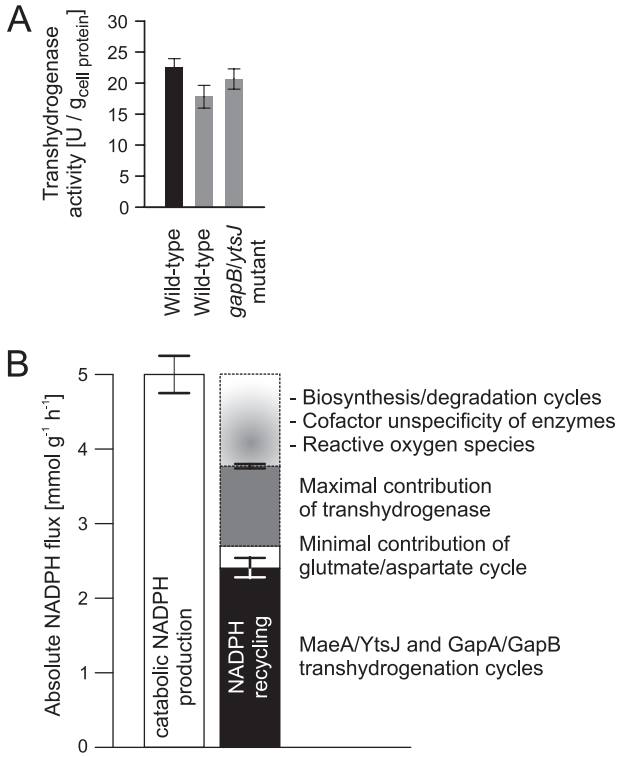

FIGURE 6. **Transhydrogenase activity (*A*) and quantification of NADPH balancing processes in nitrogen starvation-induced resting *B. subtilis* (*B*).** Transhydrogenase activity was determined in crude cell extracts of exponentially growing *B. subtilis* wild-type (*black bar*) and of resting wild-type and *ytsJ*/*gapB* double mutant (*gray bars*), where *error bars* represent technical replicates. The *error bars* on the NADPH balancing reactions represent the confidence region of the ^{13}C-flux estimates for the cycles, and the *error bars* from the *in vitro* data represent the transhydrogenase activity. *U*, units.

DISCUSSION

How growth-arrested yet metabolically active bacteria balance their network-wide NADPH redox cofactor fluxes remained unknown because NADPH production and consumption could not be quantified under such conditions. Guided by a global transcript analysis, we identified here the metabolic key mechanisms of *B. subtilis* to recycle the catabolically produced NADPH into NADH and quantified their relative contribution by a novel method for stationary ^{13}C-flux analysis (24), ^{2}H-labeling experiments, and kinetic flux profiling (28). Based on intracellular carbon flux distributions in *B. subtilis* wild-type and isogenic deletion mutants in various pathways, we propose the following model of NADPH homeostasis in nitrogen starvation-induced resting *B. subtilis* (Fig. 6*B*). Sustained metabolic activity in the absence of cell growth leads to an apparent catabolic NADPH overproduction of 5.0 ± 0.6 mmol·g^{-1}·h^{-1} that is recycled to NADH by (i) the combined activity of the MalS/YtsJ and GapA/GapB dehydrogenase isoenzyme transhydrogenation cycles, (ii) continuous cycling between anabolism and catabolism of amino acids, and (iii) a transhydrogenase reaction. In particular, the GapA/GapB transhydrogenation cycle was surprising because *gapB* was considered to be fully repressed by glucose (32, 50). The YqfL-dependent derepression of *gapB* shown here provides first indication that YqfL could be a sensor of redox imbalance that would influence *gapB* expression by inhibiting the CcpN repressor activity on *gapB*. Because transhydrogenation cycles have so far only been shown in higher cells (57, 58), we provide here the first evidence for their *in vivo* relevance in NADPH balancing of bacteria.

The individual contributions of the above three mechanisms to overall recycling of the catabolically produced NADPH in resting *B. subtilis* were ~50% for the two redox cycles, a lower bound of 6% for amino acid cycling, and ~20% for the transhydrogenase, leaving still an apparent NADPH overproduction of 1.3 ± 0.6 mmol·g^{-1}·h^{-1} unassigned (Fig. 6*B*). In principle, the substitution of the three mechanisms for each other, similar to that shown for the two redox cycles, could explain the remaining 25% of apparent NADPH overproduction, and the extent of amino acid cycling between NADPH-requiring anabolism and NADH-producing catabolism could be much larger than the lower bound of 6%. Another potential contributor to redox balancing could be NADPH consumption by detoxification of reactive oxygen species (59, 60), although our transcript data provide no indication for oxidative stress. Lastly, redox cofactor unspecificity of central metabolic enzymes (31) could reduce the amount of catabolically produced NADPH, or, although not reported so far for *B. subtilis*, a small redox cofactor unspecificity of the respiratory chain could reoxidize some of the overproduced NADPH (61).

In the absence of biosynthetic NADPH requirements, overproduction of NADPH is inevitable in resting cells that continue to catabolize sugars to CO_2. The diverse, here described redox cycling mechanisms are a stoichiometric necessity to maintain redox homeostasis in the absence of NADPH requirements for biosynthesis or redox stress. The continued metabolic activity of resting cells ensures reactivity to changing nutritional conditions, a hypothesis that would be consistent with the observation that also very slowly growing *B. subtilis* under various limitations apparently overproduce NADPH and can restore maximum growth rates as soon as the limitation is reversed (17, 45, 62, 63). The question remains, however, why nitrogen starvation-induced resting *B. subtilis* metabolism overproduces even more NADPH than would be necessary through the extensive catabolic pentose phosphate pathway fluxes rather than using exclusively the glycolytic pathway.

Acknowledgments—We thank K. Kobayashi and N. Ogasawara for generously providing B. subtilis mutants.

REFERENCES

1. Sonenshein, A. L. (2007) Control of key metabolic intersections in *Bacillus subtilis*. *Nat. Rev. Microbiol.* **5,** 917–927
2. Navarro Llorens, J. M., Tormo, A., and Martínez-García, E. (2010) Stationary phase in gram-negative bacteria. *FEMS Microbiol. Rev.* **34,** 476–495
3. Hayes, C. S., and Low, D. A. (2009) Signals of growth regulation in bacteria. *Curr. Opin. Microbiol.* **12,** 667–673
4. Hecker, M., Pané-Farré, J., and Völker, U. (2007) SigB-dependent general stress response in *Bacillus subtilis* and related gram-positive bacteria. *Annu. Rev. Microbiol.* **61,** 215–236
5. Hengge-Aronis, R. (1993) Survival of hunger and stress: The role of rpoS in early stationary phase gene regulation in *E. coli*. *Cell* **72,** 165–168
6. López, D., and Kolter, R. (2010) Extracellular signals that define distinct and coexisting cell fates in *Bacillus subtilis*. *FEMS Microbiol. Rev.* **34,** 134–149

7. Sonderegger, M., Schümperli, M., and Sauer, U. (2005) Selection of quiescent *Escherichia coli* with high metabolic activity. *Metab. Eng.* **7,** 4–9
8. Sandiford, B. R., and Wooldridge, W. R. (1931) "Resting" bacteria. *Biochem. J.* **25,** 2172–2180
9. Lewis, D. L., and Gattie, D. K. (1991) The ecology of quiescent microbes. *ASM News* **57,** 27–32
10. Vitousek, P. M., and Howarth, R. W. (1991) Nitrogen limitation on land and in the sea: How can it occur? *Biogeochemistry* **13,** 87–115
11. Luo, Y., Su, B., Currie, W. S., Dukes, J. S., Finzi, A. C., Hartwig, U., Hungate, B., McMurtrie, R. E., Oren, R., Parton, W. J., Pataki, D. E., Shaw, M. R., Zak, D. R., and Field, C. B. (2004) Progressive nitrogen limitation of ecosystem responses to rising atmospheric carbon dioxide. *BioScience* **54,** 731–739
12. Vitousek, P. M., Porder, S., Houlton, B. Z., and Chadwick, O. A. (2010) Terrestrial phosphorus limitation: Mechanisms, implications, and nitrogen-phosphorus interactions. *Ecol. Appl.* **20,** 5–15
13. Rennenberg, H., Dannenmann, M., Gessler, A., Kreuzwieser, J., Simon, J., and Papen, H. (2009) Nitrogen balance in forest soils: Nutritional limitation of plants under climate change stresses. *Plant Biol.* **11,** 4–23
14. Botella, E., Hübner, S., Hokamp, K., Hansen, A., Bisicchia, P., Noone, D., Powell, L., Salzberg, L. I., and Devine, K. M. (2011) Cell envelope gene expression in phosphate-limited *Bacillus subtilis* cells. *Microbiology* **157,** 2470–2484
15. Marzan, L. W., and Shimizu, K. (2011) Metabolic regulation of *Escherichia coli* and its phoB and phoR genes knock-out mutants under phosphate and nitrogen limitations as well as at acidic condition. *Microb. Cell Fact.* **10,** 39
16. Zamboni, N., Fischer, E., Muffler, A., Wyss, M., Hohmann, H. P., and Sauer, U. (2005) Transient expression and flux changes during a shift from high to low riboflavin production in continuous cultures of *Bacillus subtilis*. *Biotechnol. Bioeng.* **89,** 219–232
17. Dauner, M., Storni, T., and Sauer, U. (2001) *Bacillus subtilis* metabolism and energetics in carbon-limited and excess-carbon chemostat culture. *J. Bacteriol.* **183,** 7308–7317
18. Fürch, T., Hollmann, R., Wittmann, C., Wang, W., and Deckwer, W. D. (2007) Comparative study on central metabolic fluxes of *Bacillus megaterium* strains in continuous culture using ^{13}C-labeled substrates. *Bioprocess Biosyst. Eng.* **30,** 47–59
19. Sauer, U. (2006) Metabolic networks in motion: ^{13}C-based flux analysis. *Mol. Syst. Biol.* **2,** 62
20. Zamboni, N., and Sauer, U. (2009) Novel biological insights through metabolomics and ^{13}C-flux analysis. *Curr. Opin. Microbiol.* **12,** 553–558
21. Wiechert, W. (2001) ^{13}C metabolic flux analysis. *Metab. Eng.* **3,** 195–206
22. Zamboni, N., Fendt, S. M., Rühl, M., and Sauer, U. (2009) ^{13}C-based metabolic flux analysis. *Nat. Protoc.* **4,** 878–892
23. Tang, Y. J., Martin, H. G., Myers, S., Rodriguez, S., Baidoo, E. E., and Keasling, J. D. (2009) Advances in analysis of microbial metabolic fluxes via ^{13}C isotopic labeling. *Mass Spectrom. Rev.* **28,** 362–375
24. Rühl, M., Rupp, B., Nöh, K., Wiechert, W., Sauer, U., and Zamboni, N. (2012) Collisional fragmentation of central carbon metabolites in LC-MS/MS increases precision of ^{13}C metabolic flux analysis. *Biotechnol. Bioeng.* **109,** 763–771
25. Kiefer, P., Nicolas, C., Letisse, F., and Portais, J. C. (2007) Determination of carbon labeling distribution of intracellular metabolites from single fragment ions by ion chromatography tandem mass spectrometry. *Anal. Biochem.* **360,** 182–188
26. Schaub, J., Mauch, K., and Reuss, M. (2008) Metabolic flux analysis in *Escherichia coli* by integrating isotopic dynamic and isotopic stationary ^{13}C labeling data. *Biotechnol. Bioeng.* **99,** 1170–1185
27. van Winden, W. A., van Dam, J. C., Ras, C., Kleijn, R. J., Vinke, J. L., van Gulik, W. M., and Heijnen, J. J. (2005) Metabolic flux analysis of *Saccharomyces cerevisiae* CEN.PK113–7D based on mass isotopomer measurements of ^{13}C-labeled primary metabolites. *FEMS Yeast Res.* **5,** 559–568
28. Yuan, J., Bennett, B. D., and Rabinowitz, J. D. (2008) Kinetic flux profiling for quantitation of cellular metabolic fluxes. *Nat. Protoc.* **3,** 1328–1340
29. Toya, Y., Ishii, N., Hirasawa, T., Naba, M., Hirai, K., Sugawara, K., Igarashi, S., Shimizu, K., Tomita, M., and Soga, T. (2007) Direct measurement of isotopomer of intracellular metabolites using capillary electrophoresis time-of-flight mass spectrometry for efficient metabolic flux analysis. *J. Chromatogr. A* **1159,** 134–141
30. Rantanen, A., Rousu, J., Kokkonen, J. T., Tarkiainen, V., and Ketola, R. A. (2002) Computing positional isotopomer distributions from tandem mass spectrometric data. *Metab. Eng.* **4,** 285–294
31. Fuhrer, T., and Sauer, U. (2009) Different biochemical mechanisms ensure network-wide balancing of reducing equivalents in microbial metabolism. *J. Bacteriol.* **191,** 2112–2121
32. Fillinger, S., Boschi-Muller, S., Azza, S., Dervyn, E., Branlant, G., and Aymerich, S. (2000) Two glyceraldehyde-3-phosphate dehydrogenases with opposite physiological roles in a nonphotosynthetic bacterium. *J. Biol. Chem.* **275,** 14031–14037
33. Nicolas, P., Mäder, U., Dervyn, E., Rochat, T., Leduc, A., Pigeonneau, N., Bidnenko, E., Marchadier, E., Hoebeke, M., Aymerich, S., Becher, D., Bisicchia, P., Botella, E., Delumeau, O., Doherty, G., Denham, E. L., Fogg, M. J., Fromion, V., Goelzer, A., Hansen, A., Härtig, E., Harwood, C. R., Homuth, G., Jarmer, H., Jules, M., Klipp, E., Le Chat, L., Lecointe, F., Lewis, P., Liebermeister, W., March, A., Mars, R. A., Nannapaneni, P., Noone, D., Pohl, S., Rinn, B., Rügheimer, F., Sappa, P. K., Samson, F., Schaffer, M., Schwikowski, B., Steil, L., Stülke, J., Wiegert, T., Devine, K. M., Wilkinson, A. J., van Dijl, J. M., Hecker, M., Völker, U., Bessières, P., and Noirot, P. (2012) Condition-dependent transcriptome reveals high-level regulatory architecture in *Bacillus subtilis*. *Science* **335,** 1103–1106
34. Rasmussen, S., Nielsen, H. B., and Jarmer, H. (2009) The transcriptionally active regions in the genome of *Bacillus subtilis*. *Mol. Microbiol.* **73,** 1043–1057
35. Nicolas, P., Leduc, A., Robin, S., Rasmussen, S., Jarmer, H., and Bessières, P. (2009) Transcriptional landscape estimation from tiling array data using a model of signal shift and drift. *Bioinformatics* **25,** 2341–2347
36. Wiechert, W., Schweissgut, O., Takanaga, H., and Frommer, W. B. (2007) Fluxomics: Mass spectrometry versus quantitative imaging. *Curr. Opin. Plant Biol.* **10,** 323–330
37. de Koning, W., and van Dam, K. (1992) A method for the determination of changes of glycolytic metabolites in yeast on a subsecond time scale using extraction at neutral pH. *Anal. Biochem.* **204,** 118–123
38. Wiechert, W., Möllney, M., Petersen, S., and de Graaf, A. A. (2001) A universal framework for ^{13}C metabolic flux analysis. *Metab. Eng.* **3,** 265–283
39. Kleijn, R. J., Buescher, J. M., Le Chat, L., Jules, M., Aymerich, S., and Sauer, U. (2010) Metabolic fluxes during strong carbon catabolite repression by malate in *Bacillus subtilis*. *J. Biol. Chem.* **285,** 1587–1596
40. Zamboni, N., Fischer, E., Laudert, D., Aymerich, S., Hohmann, H. P., and Sauer, U. (2004) The *Bacillus subtilis* yqjI gene encodes the NADP$^+$-dependent 6-P-gluconate dehydrogenase in the pentose phosphate pathway. *J. Bacteriol.* **186,** 4528–4534
41. Lerondel, G., Doan, T., Zamboni, N., Sauer, U., and Aymerich, S. (2006) YtsJ has the major physiological role of the four paralogous malic enzyme isoforms in *Bacillus subtilis*. *J. Bacteriol.* **188,** 4727–4736
42. Maier, K., Hofmann, U., Reuss, M., and Mauch, K. (2008) Identification of metabolic fluxes in hepatic cells from transient ^{13}C-labeling experiments: Part II. Flux estimation. *Biotechnol. Bioeng.* **100,** 355–370
43. Munger, J., Bennett, B. D., Parikh, A., Feng, X. J., McArdle, J., Rabitz, H. A., Shenk, T., and Rabinowitz, J. D. (2008) Systems-level metabolic flux profiling identifies fatty acid synthesis as a target for antiviral therapy. *Nat. Biotechnol.* **26,** 1179–1186
44. Nöh, K., Grönke, K., Luo, B., Takors, R., Oldiges, M., and Wiechert, W. (2007) Metabolic flux analysis at ultra short time scale: Isotopically non-stationary ^{13}C labeling experiments. *J. Biotechnol.* **129,** 249–267
45. Rühl, M., Zamboni, N., and Sauer, U. (2010) Dynamic flux responses in riboflavin overproducing *Bacillus subtilis* to increasing glucose limitation in fed-batch culture. *Biotechnol. Bioeng.* **105,** 795–804
46. Mostertz, J., Scharf, C., Hecker, M., and Homuth, G. (2004) Transcriptome and proteome analysis of *Bacillus subtilis* gene expression in response to superoxide and peroxide stress. *Microbiology* **150,** 497–512
47. Eymann, C., Homuth, G., Scharf, C., and Hecker, M. (2002) *Bacillus subtilis* functional genomics: Global characterization of the stringent response by proteome and transcriptome analysis. *J. Bacteriol.* **184,** 2500–2520
48. Tam le, T., Eymann, C., Antelmann, H., Albrecht, D., and Hecker, M. (2007) Global gene expression profiling of *Bacillus subtilis* in response to

ammonium and tryptophan starvation as revealed by transcriptome and proteome analysis. *J. Mol. Microbiol. Biotechnol.* **12,** 121–130
49. Servant, P., Le Coq, D., and Aymerich, S. (2005) CcpN (YqzB), a novel regulator for CcpA-independent catabolite repression of *Bacillus subtilis* gluconeogenic genes. *Mol. Microbiol.* **55,** 1435–1451
50. Tännler, S., Fischer, E., Le Coq, D., Doan, T., Jamet, E., Sauer, U., and Aymerich, S. (2008) CcpN controls central carbon fluxes in *Bacillus subtilis*. *J. Bacteriol.* **190,** 6178–6187
51. Licht, A., Preis, S., and Brantl, S. (2005) Implication of CcpN in the regulation of a novel untranslated RNA (SR1) in *Bacillus subtilis*. *Mol. Microbiol.* **58,** 189–206
52. Zhang, B. L., Yunianta, and Martin, M. L. (1995) Site-specific isotope fractionation in the characterization of biochemical mechanisms. The glycolytic pathway. *J. Biol. Chem.* **270,** 16023–16029
53. Roger, O., Lavigne, R., Mahmoud, M., Buisson, C., Onno, B., Zhang, B. L., and Robins, R. J. (2004) Quantitative ^{2}H NMR at natural abundance can distinguish the pathway used for glucose fermentation by lactic acid bacteria. *J. Biol. Chem.* **279,** 24923–24928
54. Sauer, U., Canonaco, F., Heri, S., Perrenoud, A., and Fischer, E. (2004) The soluble and membrane-bound transhydrogenases UdhA and PntAB have divergent functions in NADPH metabolism of *Escherichia coli*. *J. Biol. Chem.* **279,** 6613–6619
55. Bergsma, J., Van Dongen, M. B., and Konings, W. N. (1982) Purification and characterization of NADH dehydrogenase from *Bacillus subtilis*. *Eur. J. Biochem.* **128,** 151–157
56. Dauner, M., and Sauer, U. (2001) Stoichiometric growth model for riboflavin-producing *Bacillus subtilis*. *Biotechnol. Bioeng.* **76,** 132–143
57. Comte, B., Vincent, G., Bouchard, B., Benderdour, M., and Des Rosiers, C. (2002) Reverse flux through cardiac NADP^{+}-isocitrate dehydrogenase under normoxia and ischemia. *Am. J. Physiol. Heart Circ. Physiol.* **283,** H1505–1514
58. Overkamp, K. M., Bakker, B. M., Steensma, H. Y., van Dijken, J. P., and Pronk, J. T. (2002) Two mechanisms for oxidation of cytosolic NADPH by *Kluyveromyces lactis* mitochondria. *Yeast* **19,** 813–824
59. Lushchak, V. I. (2011) Adaptive response to oxidative stress: Bacteria, fungi, plants, and animals. *Comp. Biochem. Physiol. C Toxicol. Pharmacol.* **153,** 175–190
60. Mailloux, R. J., Lemire, J., and Appanna, V. D. (2011) Metabolic networks to combat oxidative stress in *Pseudomonas fluorescens*. *Antonie Van Leeuwenhoek* **99,** 433–442
61. Auriol, C., Bestel-Corre, G., Claude, J. B., Soucaille, P., and Meynial-Salles, I. (2011) Stress-induced evolution of *Escherichia coli* points to original concepts in respiratory cofactor selectivity. *Proc. Natl. Acad. Sci. U.S.A.* **108,** 1278–1283
62. Sauer, U., Hatzimanikatis, V., Bailey, J. E., Hochuli, M., Szyperski, T., and Wüthrich, K. (1997) Metabolic fluxes in riboflavin-producing *Bacillus subtilis*. *Nat. Biotechnol.* **15,** 448–452
63. Tännler, S., Decasper, S., and Sauer, U. (2008) Maintenance metabolism and carbon fluxes in *Bacillus* species. *Microb. Cell Fact.* **7,** 19
64. Buescher, J. M., Liebermeister, W., Jules, M., Uhr, M., Muntel, J., Botella, E., Hessling, B., Kleijn, R. J., Le Chat, L., Lecointe, F., Mäder, U., Nicolas, P., Piersma, S., Rügheimer, F., Becher, D., Bessieres, P., Bidnenko, E., Denham, E. L., Dervyn, E., Devine, K. M., Doherty, G., Drulhe, S., Felicori, L., Fogg, M. J., Goelzer, A., Hansen, A., Harwood, C. R., Hecker, M., Hubner, S., Hultschig, C., Jarmer, H., Klipp, E., Leduc, A., Lewis, P., Molina, F., Noirot, P., Peres, S., Pigeonneau, N., Pohl, S., Rasmussen, S., Rinn, B., Schaffer, M., Schnidder, J., Schwikowski, B., Van Dijl, J. M., Veiga, P., Walsh, S., Wilkinson, A. J., Stelling, J., Aymerich, S., and Sauer, U. (2012) Global network reorganization during dynamic adaptations of *Bacillus subtilis* metabolism. *Science* **335,** 1099–1103
65. Ferguson, M. L., Le Coq, D., Jules, M., Aymerich, S., Declerck, N., and Royer, C. A. (2011) Absolute quantification of gene expression in individual bacterial cells using two-photon fluctuation microscopy. *Anal. Biochem.* **419,** 250–259